Method Development for Experimental Characterization of Dynamic Strength of Aluminum Structures

Natalie Schaal[1], Peter Bishay[1], Erik Serrano[1], and J. Brent Knight[2]

[1] Department of Mechanical Engineering
California State University, Northridge, CA 91330

[2] Space Systems Department Optical Systems Design and Fabrication Branch
NASA Marshall Space Flight Center, Huntsville, AL, 35808

ABSTRACT
Space Flight Hardware (SFH) experiences intense vibratory loading during flight, which only lasts a few minutes. When determining the appropriate size of these components to withstand such loading without becoming damaged, standard design practice is to assume that the peak dynamic loads are applied statically. In doing so, the resulting stress is compared against a material strength parameter obtained from a quasi-static experiment. Since the near-peak stresses are only experienced over a small fraction of time in reality, this approach leads to design conservatism that unnecessarily increases structural mass as well as the associated inefficiency and financial cost.

In an effort to modernize engineering design standards to appropriately consider the higher practical strength of dynamically loaded structures, this overarching research project seeks to develop an experimental test procedure for quantifying the dynamic strength of metallic alloys as a function of excitation frequency. In the ideal case, the characterization test would include an in-situ method for monitoring the onset and progression of plastic deformation of the test specimen undergoing vibratory loading. These new tests are designed to be high intensity (forcing amplitude), short term (60 seconds at full amplitude), and cyclic in nature (sinusoidal excitation via attached stinger to an otherwise cantilevered beam). In addition, the initial alloy under investigation is 6061 aluminum, due to its wide use and applicability for SFH.

Thus far, the primary candidate under development with live-capacity is to track hysteresis behavior of the beam from power dissipation trends, calculated via force (from transducer on excitation stinger) and velocity (measurements from Laser Doppler Vibrometer) data and work to distinguish between elastic and plastic features. As a key component of this ongoing method development, any pseudo-live indication of plasticity could be corroborated against the outcome of a pre-post assessment of damage via macroscopic evaluation of beam geometry (i.e. assessing any permanent change in the beam's tip deflection). Support for experimental design decisions as well as dynamic strength data from tests with excitation frequencies of 10, 40, and 55 Hz will be discussed. This work contributes to the foundation for a new type of vibration-based characterization experiments and generates initial data on the functional strength of 6061 aluminum under the conditions considered.

Keywords: vibrations, plastic deformation, aluminum, dynamic, testing

INTRODUCTION

The motivation for this work is provided by vibration tests of a cantilevered 6063 aluminum beam performed by NASA Marshal Space Center (MSFC) in 2019 that produced response displacements much greater than those observed in a static test of the same beam design [1]. The static displacement was approximately 1 in (2.54 cm) and resulted in visibly clear plastic deformation. The sine dwell vibration test tip displacements were estimated to be +/- 6 in (15.24 cm), after which no visible fracture or plastic deformation resulted [1]. This observation merits questioning the conservatism in the longstanding design practice of assuming or treating the applied load as completely static when stress analyses are performed to size the hardware. This "static standard" is taught to current engineering students from all typical machine design textbooks, including Shigley [2]. Moreover, NASA's technical standards handbooks [3-4] also assert the use of statically measured

strength parameters (e.g., yield and ultimate strengths) in designing mechanical components and flight structures that experience dynamic/cyclic loads. The continued use of this deep-rooted static-based design approach appears to be due to the lack of an innovative and applicable alternative. Moreover, the consequences of this hypothesized and unintentional high level of conservatism include, but are not limited to, higher weight, fuel consumption, and costs.

Any proposed new or modified design approach has to be a quick turnaround process to have utility in any schedule-driven engineering development effort. A material "dynamic strength" associated with limited load cycles and as a function of frequency, if one could be developed and vetted, would serve that purpose. This paper presents first efforts to devise a way to measure such a hypothesized strength property and start collecting data for one aluminum alloy used regularly in Space Flight Hardware (SFH): 6061 aluminum. In particular, the scope of this work is to develop an experimental test procedure for determining how much higher the dynamic failure load (for a fixed frequency, fixed duration, low-cycle test) could be than the true static critical load. Highlights from the scientific exploration are given and results thus far in assessing the behavior of 6061 aluminum beams under the considered conditions are presented.

BACKGROUND

When considering "strength" under vibratory loads in general, the standard of practice is to estimate the lifetime of a structural material via fatigue testing, in which specimens are subjected to constant-frequency, constant-magnitude, cyclic loading until failure. These tests are performed on many specimens at different amplitudes to construct the S-N diagram that shows how increasing the amplitude of vibration decreases the fatigue life of the material being tested. As these types of tests are typically categorized as Low Cycle Fatigue (LCF, high amplitude, stress exceeding static yield strength, low fatigue life) or High Cycle Fatigue (HCF, low amplitude, stress below static yield strength, high fatigue life) [5], a knowledge gap remains in the literature for mid-way stresses. In addition, another knowledge gap appears to exist for non-fatigue testing, i.e. short-term instead of long-term cyclic loading. Exploring the potential dynamic strength gains (instead of the fatigue life) could be an untapped avenue of research. In-situ monitoring and detection of plastic deformation initiation in the vibrating specimens, as explored in this project, also appears to not be a commonly available technology.

In order to experimentally explore the failure (yielding) of aluminum under cyclic loading, a method for detecting the onset or progression of plastic deformation is needed. An in-situ method would be ideal. Changes in energy loss or power dissipation due to plastic deformation has been a primary candidate for a monitoring method in this work. In addition, it is well known that all structures in motion dissipate energy at least due to internal material friction [6]. The source of energy loss may produce a different hysteresis behavior as seen, for example, in the shape of force-deflection loops (i.e. for material vs. dry friction vs. viscous damping) [6]. There is also evidence that the frequency dependence of damping may differ as a function of the physical source of damping [7] and aluminum has rate-dependent plasticity (visco-plasticity) behavior [8-9]. The onset of plastic deformation resulting in a change of power dissipated per cycle or a change in the hysteresis behavior is being explored and the investigation is ongoing.

METHODOLOGY

In addition to tracking of the force-velocity hysteresis curves and power dissipation, a few other approaches with live-capacity were conceptually and experimentally explored, including Digital Image Correlation (DIC) to determine plastic strain, and monitoring local temperature changes from plastic deformation. While the image-based method was later halted due to camera limitations, the temperature monitoring method is in development and will be discussed in a future publication. The second method presented in the current paper for determining the existence and extent of plastic deformation arising from cyclic dynamic loading in the fixed-duration tests is to compare the pre-/post-test permanent tip deflection. For the sake of brevity, the permanent tip deflection is abbreviated as PTD, and the magnitude of any pre-/post-test change is referenced as ΔPTD, as defined below in equation (1).

$$\Delta\mathrm{PTD} = \left|\mathrm{PTD}_{post} - \mathrm{PTD}_{pre}\right| \tag{1}$$

The excitation in the dynamic tests is provided by a 489 N electrodynamic shaker (The Modal Shop: model 2110E, 489 N, 25.4 mm peak-to-peak stroke) with accompanying power amplifier (model 250E09-FS). Due to the practical restrictions created by balancing the interest of testing beams of significant size (in this case, 12 in / 30.48 cm total length, 1 in / 2.54 cm width, and 1/16 in / 0.159 cm thickness) at forces much higher than the static failure load, all while protecting the shaker from loading imbalances that could cause internal damage, a stinger-type (The Modal Shop: model 2155G12, steel) approach to excite an otherwise cantilevered beam was chosen over a classic base-excitation scenario. A piezoelectric transducer (PCB Piezotronics: model 208C02) threaded onto the stinger tip was used to measure applied force. Multipurpose 6061-T6 aluminum beams were purchased with the following as-manufactured geometric tolerances: +/- 0.006 in (0.0152 cm) on thickness, +/-0.014 in (0.0356 cm) on width. A custom experimental set up was designed and manufactured, including a custom clamp with over-designed M14 bolts to hold the cantilevered beam in place. A plexiglass safety shield was also designed and manufactured to protect both people and equipment from damage in the case that a beam catastrophically failed during a test. Along with a Laser Doppler Vibrometer (LDV) (Polytec: model PSV-500-HV Scanning Vibrometer), the 489 N electrodynamic shaker and the rest of the set up was arranged on top of an optical table. A schematic and picture of the actual set up is shown in Figure 1 below.

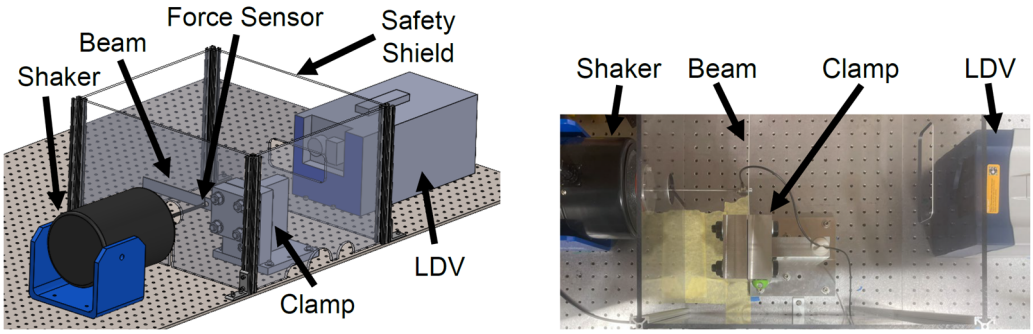

Fig. 1 Diagrams of test set up for dynamic experiments performed on cantilvered aluminum beam

Within the large clamp that holds the beam with four M14 bolts, two pins help to orient the beam. Of the 12-inch (30.48-cm) beams, 3 inches (7.62 cm) is sandwiched within the clamp, leaving 9 inches (22.86 cm) of the beam exposed to deflect during the dynamic test. During the setup portion of the procedure, a water level is used to ensure that the beam is oriented horizontally. The force sensor is threaded onto the stinger and then attached to the beam 2 inches (5.08 cm) away from the edge of the clamp (i.e. 7 inches / 17.78 cm away from the free end of the beam). On the opposite face, the laser point from the LDV is located approximately 1.5 inches (3.81 cm) away from the clamp, in the middle of the beam's width. The three holes (two pin holes and one hole for the screw to secure the force sensor) in the beam were manufactured in-house at CSUN's machine shop.

These dynamic characterization tests are designed to be high intensity (in terms of forcing amplitude), short term (60 seconds at full amplitude), and cyclic in nature (sinusoidal excitation). The full dynamic test is 70 seconds long, which includes 64 seconds of excitation composed of a tukey (tapered cosine) windowed sine wave with a 2-second ramp up and 2-second ramp down on either side of 60 seconds of full amplitude signal. The remaining 6 seconds is a cool-down period of zero excitation. MATLAB was used to generate the windowed excitation signal at the desired frequency, and custom Python code was used to communicate with the Polytec software to utilize this custom signal and internally trigger the measurement. The excitation signal was chosen to be windowed to minimize any impulsive effects that may arise from the otherwise sudden starting or stopping of the test, and the length of the full amplitude excitation segment was motivated by the duration of typical random vibration flight acceptance tests typically lasting 60 seconds. A sinusoidal excitation was chosen over random vibration because it is typically harsher on the part. An example of the realized forcing as a function of time as measured by the force sensor on the tip of the stinger is shown in Figure 2 of the Results & Discussion section, for a 10 Hz case with an intended forcing amplitude of 75 N (run with beam ID 10_7).

As previously indicated, prior to the dynamic test, the PTD_{pre} (pre-test permanent tip deflection) is measured. In terms of setup, this is done on a flat cast iron plate, using a soft clamp to mimic the dynamic test setup by clamping the beam at the

same location as the large-scale test clamp (i.e. with the side of the soft clamp aligned such that 9 in / 22.86 cm of the beam is still free). A height gage (iGaging: model 35-630, precision 0.01 microns, accuracy 0.04 mm) is placed next to the free end of the beam, zeroed to the surface of the plate, and then carefully used to measure the top height of the tip of the beam. The tip thickness, averaged from three measurements using a flat-head micrometer (Mitutoyo: model 70538897, precision 0.0010 mm, accuracy 0.0010 mm**)** at the beam tip is subtracted from this height, generating the gap between the top of the plate and the bottom of the beam tip: PTD_{pre}. As it is important for accuracy of the measurement that the bottom of the height gage indicator only gently touches the top of the beam, without pushing the beam down and thereby obscuring the actual PTD, this measurement was taken by two test engineers (one faculty and one student) and refined until agreement was reached. After the dynamic test, the beam is returned to the cast iron plate and the PTD is measured again, producing the PTD_{post} (post-test PTD). This cast iron plate has a known surface variation of approximately +/-1 thousandths of an inch, which is +/- 0.0254 mm. As the height gage is zeroed to the plate just beyond the beam's tip before taking a measurement, for the sake of this initial study, a ΔPTD equal to or greater than 0.05 mm was interpreted to mean that plastic deformation occurred during the dynamic test. Until a full analysis of the sources and extent of the error is conducted, this interim threshold is used, albeit as a soft or open threshold when it comes to discussion.

During each dynamic test, the sampling frequency of 5 kHz was used for the LDV and force sensor measurements. The surface velocity of the beam at the targeted point as a function of time was recorded from the LDV, along with the applied force from the stinger onto the beam as a function of time from the force sensor. In addition, the temperature and humidity of the room was logged for each test, which ranged from 23.7 °C to 28.1 °C with a median of 26.5 °C for the room temperature, and ranged from 25% to 56% with a median of 41% for the room humidity. For any case where the beam visibly fractured, the test was stopped early to prevent damage to the equipment.

Test cases were designed based on a calculated and test-verified value of the critical applied force that would cause a beam of the same material properties and geometry to fail under a static load. The theoretical static failure load was calculated via the well-known yield equation from max bending stress of $F_Y = (2I\sigma_Y)/(ha)$, where I is the area moment of inertia for the beam's cross-section, σ_Y is the yield strength, h is the height of the beam (thickness), and a is the distance from the fixture to the load application point (at stinger / force sensor attachment) [2], using a yield strength of 241 MPa from the manufacturer, which came out to be 50.6 N. In addition, a small series of static tests were conducted on beams from the same manufacturer to check the theoretical value in practice. These static confirmation tests were performed on beams with the same amount of exposed beam length of 9 in (22.86 cm) and held in the clamp from the large-scale setup. A dead-weight style load was applied through a wire and pully system, running horizontally through the same stinger hole as for the dynamic tests. Static failure was interpreted by visually analyzing any noticeable change in the unloaded tip location of the beam using a downward projected camera and a flat grid with resolution of 2 mm (cell size) positioned directly under the beam. From this procedure, the static failure load was 46.5, 49.4, and 51.4 N across three beams, which is generally consistent with the theoretical value. Approximating the representative value to be a rounded 50 N, the baseline dynamic tests were designed to be in multiples of the static threshold, so 50 N (1x), 100 N (2x), and 150 N (3x). In addition, a clearly elastic control case of 30 N (i.e. well below the static critical load) was included. After the dynamic failure window was identified from the baseline tests, two rounds of a Bisection approach were applied to begin isolating the strength limit for a given excitation frequency. Due to the lack of a force controller and the nonlinear relationship in the trend of input voltage to applied force due to system interactions, the bisecting was applied directly to the input voltage (which, in turn, only approximately bisects the applied force). For every case, a minimum of three repeated tests were carried out to produce a reliable data set (the only exception to this repeat rule is the 10 Hz 150 N case: only one test was run, but the beam fractured).

RESULTS & DISCUSSION

As previously discussed, the focus of this study is to develop and perform dynamic tests at applied forces higher than the static failure load to explore the frequency-dependent practical strength of 6061 aluminum beams under the conditions considered. Due to the fundamental concept of resonance, forcing the beam near one of its natural frequencies would result in a low applied force, due to the characteristic self-excitation effect of resonance. As such, taking this and interactions of the shaker-stinger-beam system into account, the current excitation frequencies of interest thus far are sufficiently far away from the system's resonances and thereby allow for a relatively high applied force within the voltage input limitations of the

amplifier are 10 Hz, 40 Hz, and 55 Hz. In this paper, results from 63 full-scale completed runs are presented: 20 at 10 Hz, 19 at 40 Hz, and 24 at 55 Hz.

For efficiency, a MATLAB code was created to read the force-versus-time and velocity-versus-time data from the generated dynamic testing data files of all beams and to perform various analyses. Figure 2 shows the time history plot of the force signal for one of the beams tested at 10 Hz with intended force amplitude of 75 N (beam ID 10_7), which is higher than the critical static load to initiate plastic deformation (approx. 50 N).

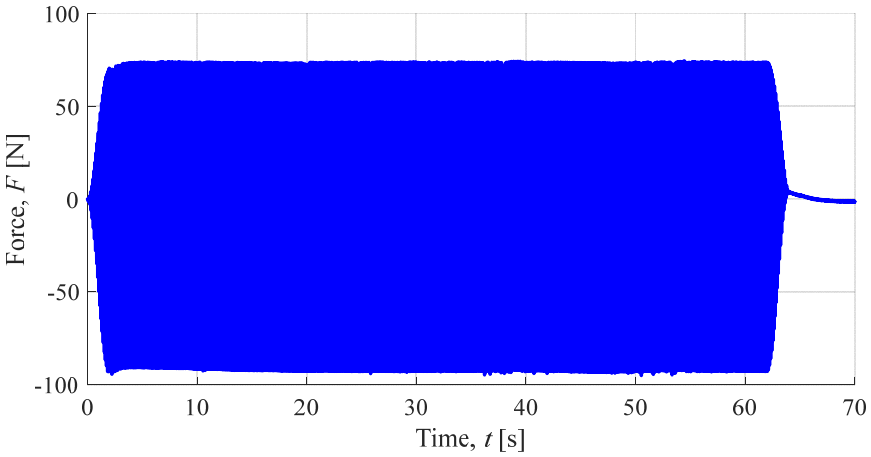

Fig. 2 Measured applied force for an entire 70-second dynamic test for beam 10_7, loaded with intended force amplitude of 75 N at 10 Hz

Figure 3 is a zoom-in view of the force and velocity signals during the first five cycles in the twenty-fifth second after the initial transient period, as an example (arbitrary "middle" temporal location), for the three beams tested at 10 Hz with intended force amplitude of 75 N (i.e. 10 Hz, 75 N case). The measured signals are plotted against the relative time, t_r, which is defined in equation (2), with t_i and t_f as the initial and final times in the data range of the plot.

$$t_r = \frac{t - t_i}{t_f - t_i} \tag{2}$$

For each beam in this case, all cycles between the ramps look similar, and the peak value is approximately the same for all cycles. Comparing the response of multiple (repeated) beams, the slight differences in the peak values indicate slight beam-to-beam variation (e.g., in the beam geometry, beam integrity or properties, or manually implemented setup).

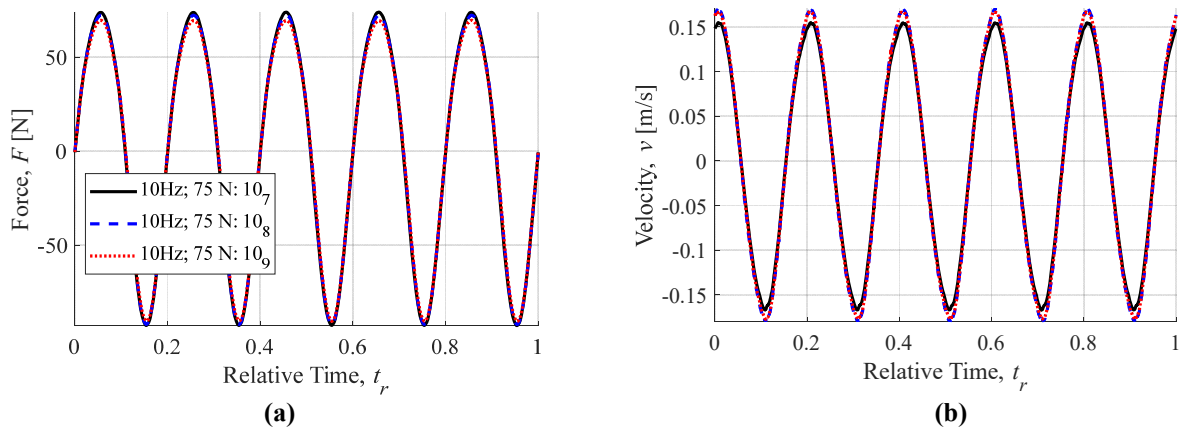

Fig. 3 Force (a) and velocity (b) vs relative time for beams loaded with intended force amplitude of 75 N at 10 Hz: first 5 cycles in the 25th second after the initial transient period

As shown in Figure 3, it is interesting to note that the maximum force measured for these cases is close to 72 N while the minimum is about -90 N. This means that, while the beam oscillates, the compressive force measured by the force transducer when the stinger pushes the beam away from the shaker is higher in magnitude than the tensile force measured when the stinger pulls the beam towards the shaker. This "negative bias" offset in the force is also depicted in Figure 2 and was observed for all dynamic tests.

To facilitate qualitative comparison between cases, repeated runs, and data types, the relative force and relative velocity, defined in equation (3) are used. $F_{max\text{-}cyc}$ and $v_{max\text{-}cyc}$ are the maximum values of the force and velocity signals in the considered cycles of the plot, respectively. The velocity versus force plots for the three highlighted 10 Hz beams for the same five cycles discussed above, in both absolute and relative sense, are shown in Figure 4. While these hysteresis traces are close to each other, any deviation indicates beam-to-beam or run-to-run variation, despite consistent procedures and excitation.

$$F_r = \frac{F}{F_{max-cyc}}; \qquad v_r = \frac{v}{v_{max-cyc}} \tag{3}$$

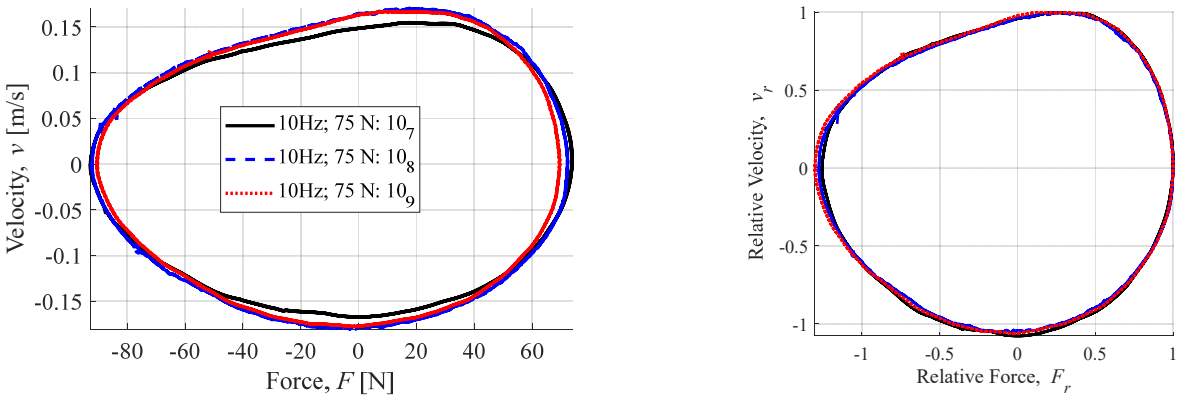

Fig. 4 Absolute velocity vs absolute force (a), relative velocity vs relative force (b), for three highlighted beams loaded with intended force amplitude of 75 N at 10 Hz: first 5 cycles in the 25th second after the initial transient period

As in Figure 4 (b), plotting relative velocity versus relative force facilitates comparison of the hysteresis loop shape. If the motion of the beam followed a perfect sine wave, then the shape of this loop should be a perfect circle. As shown, these traces follow a warped ellipse. While these cases were deemed to be elastic based on the interim ΔPTD threshold of 0.05 mm, factors that generated this shape could include the aforementioned negative bias effect or any other nonlinear or nonsymmetric effects in the system's actuation of the excitation or the geometry of the setup. While these traces are close to each other, it appears that the beam-to-beam variation is higher than the cycle-to-cycle variation for these runs and this five-cycle window.

Figure 5 shows the realized vs intended applied forcing amplitudes (F vs F_i) for all included runs at 10 and 40 Hz (38 beams). The 55 Hz cases had a similar trend and were omitted here for brevity. In most cases, the realized forcing amplitudes were close to the intended forcing amplitudes. The maximum, minimum, mean, and alternating forces used in the plot are the mean values of the respective per-cycle quantities (i.e. the mean of $F_{max\text{-}cyc}$, $F_{min\text{-}cyc}$, $F_{mean\text{-}cyc}$, $F_{alt\text{-}cyc}$, respectively), where the last two are defined in equation (4) below. The error bars in the plot represent +/- one standard deviation from the mean values.

$$F_{mean-cyc} = \frac{F_{max-cyc} + F_{min-cyc}}{2}; \qquad F_{alt-cyc} = \frac{F_{max-cyc} - F_{min-cyc}}{2} \tag{4}$$

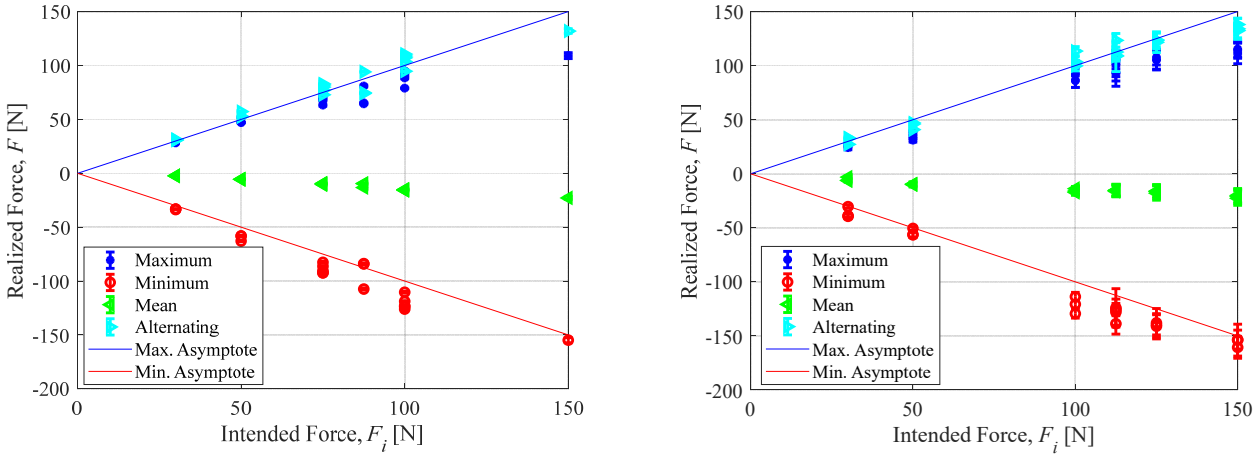

Fig. 5 Realized versus intended forces for beams excited at 10 Hz (a) and 40 Hz (b). Markers indicate the mean of the per-cycle values for a given run. Error bars represent +/- one standard deviation in the per-cycle values, and the maximum and minimum "asymptote" lines represent a one-to-one relationship between intended and realized force, for comparison

Figure 5 serves to summarize the outcomes of each run for a given excitation frequency with regards to different parameters. The aforementioned negative bias can be seen both in the per-cycle mean force (green triangles) being generally below 0, and in the minimum force (red circles) typically being below the one-to-one realized force to intended force line. With regards to the vertical axis, these data points all together show the span (of the mean) of realized forces applied to the beam at the stinger attachment location during each test. Note also that the length of the error bars increased for the 40 Hz cases (Figure 5b) as compared to the 10 Hz cases (Figure 5a), which indicates more variation in the applied forces. This variation is also more pronounced for higher intended forces.

Since all beams experienced higher negative (i.e. minimum) forces than positive (i.e. maximum) forces, it follows that the absolute value of the minimum value of $F_{min\text{-}cyc}$, called $|F_{min}|$ hereafter, represents the highest forcing amplitude that the beam experienced during the loading duration for a given run. Figure 6 shows the change in the permanent tip deflection, ΔPTD versus $|F_{min}|$ for all beams tested at 10, 40, and 55 Hz. The dashed horizontal line at 0.05 mm represents the interim plasticity threshold, above which the beam has likely experienced plastic deformation.

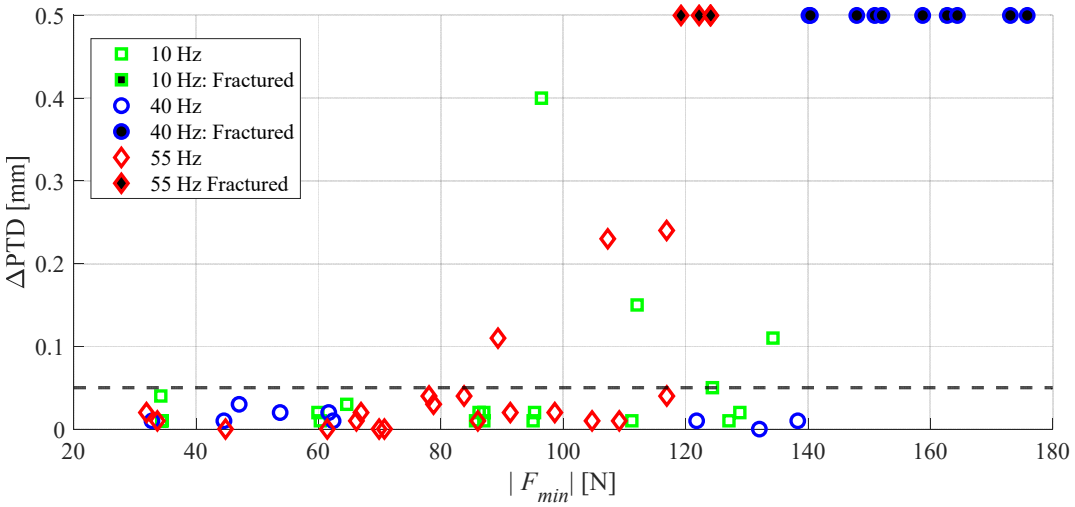

Fig. 6 Change in permanent tip deflection (i.e. ΔPTD) versus $|F_{min}|$ for all beams excited at 10, 40, and 55 Hz. The horizontal black dashed line represents the interim plasticity threshold of 0.05 mm with respect to PTD. Markers are colored by excitation frequency and any beams that fractured during the dynamic test are indicated by black-filled markers

As shown in Figure 6, the first case of plastic deformation happened when $|F_{min}| \approx 89$ N at 55 Hz. Interestingly, this force would lead to a significant permanent tip deflection if applied statically, as this force is 178% of the critical static load (approx. 50 N), supporting the concept of a practically higher dynamic strength under certain conditions. The first case in this set that fractured was for 55 Hz when $|F_{min}| = 119$ N (or 238% of the critical static load). Given the concept of fatigue life, the observation of lowest failure load for the highest frequency tested so far (55 Hz) is interpreted to be due to more cycles experienced in the same time period. It is suspected that any dynamic strength trend as a function of excitation frequency is nonlinear and may have a peak.

In an effort to summarize the outcomes from the dynamic testing in this study to date, Table 1 provides the case parameters (excitation frequency and intended force) along with the number of tests ran for each case (run count), the "plastic" vs. "elastic" outcomes based on the interim threshold of 0.05 mm (columns five through seven), and representative mean, alternating, and minimum (i.e. maximum negative) forces across all runs for each case (columns eight through ten).

Table 1 Summary of outcomes for all beams tested in this study. The first column provides the range of beam identifiers included for the data given in that row. The second and third columns provide the excitation frequency and intended force for that testing case. The fourth column displays the number of repeated tests (i.e. runs) with identical intended excitation conditions. The fifth and six columns provide a breakdown of how many of these tests produced a measured change in permanent tip deflection over the interim threshold of 0.05 mm (i.e. designated as "plastic") or under the interim threshold (i.e. designated as "elastic"). The seventh column serves to summarize the previous two columns by assigning a classification using the following symbol key: "O" means all runs were deemed elastic (i.e. below ΔPTD interim threshold), "~O" means majority of runs were deemed elastic, "~X" means the majority of runs were deemed plastic (i.e. above ΔPTD interim threshold or fractured), "XX" means all runs fractured. The eighth column provides the median value across all runs in a given case (row) of the per-run median of the per-cycle mean force F_{mean}, as calculated in equation 4. Similarly, the ninth column provides the median value across all runs in a given case (row) of the per-run median of the per-cycle alternating force F_{alt}, as calculated in equation 4. The final column gives the minimum value across all runs in a given case (row) of the minimum per-run force (i.e. the most negative) measured

Beam ID range	Excitation frequency [Hz]	Intended force [N]	Run count	Run count with ΔPTD > 0.05 mm or fractured	Run count with ΔPTD < 0.05 mm	Case outcome	Median of F_{mean} [N]	Median of F_{alt} [N]	Min of F_{min} [N]
10_1-10_3	10	30	3	0	3	O	-2.4	30.9	-34.4
10_4-10_6	10	50	3	0	3	O	-5.6	52.7	-64.2
10_7-10_{11}	10	75	5	1	4	~O	-9.7	80.0	-96.4
10_{12}-10_{14}	10	87.5	3	0	3	O	-9.7	74.8	-111.2
10_{15}-10_{19}	10	100	5	3	2	~X	-15.5	107.2	-134.3
10_{20}	10	150	1	1	0	XX	-22.5	132.8	-162.9
40_1-40_3	40	30	3	0	3	O	-5.9	32.7	-46.2
40_4-40_6	40	50	3	0	3	O	-9.7	46.3	-61.7
40_7-40_9	40	100	3	0	3	O	-15.6	105.3	-138.3
40_{10}-40_{13}	40	112.5	4	3	1	~X	-15.0	115.0	-152.1
40_{14}-40_{16}	40	125	3	3	0	XX	-16.9	125.5	-164.4
40_{17}-40_{19}	40	150	3	3	0	XX	-22.0	136.9	-175.8
55_1-55_3	55	30	3	0	3	O	-3.7	27.3	-44.8
55_4-55_6	55	50	3	0	3	O	-6.1	55.4	-69.9
55_7-55_{10}	55	62.5	4	0	4	O	-9.0	53.2	-78.8
55_{11}-55_{15}	55	75	5	2	3	~O	-9.5	69.3	-107.3
55_{16}-55_{20}	55	87.5	5	1	4	~O	-10.5	91.6	-116.9
55_{21}-55_{24}	55	100	4	4	0	XX	-12.3	102.1	-124.1

At this stage in the ongoing study, the transition between an elastic or mostly elastic case (indicated by a "O" or "~O" symbol in the table, respectively) to a mostly plastic or fractured case (indicated by a "~X" or "XX" symbol in the table, respectively) is estimated to be the approximate window in which the "dynamic strength" lies. Currently, with respect to the intended forces, these windows are 87.5-100 N for 10 Hz, 100-112.5 N for 40 Hz, and 87.5-100 N for 55 Hz. Based on an approximate static failure load of 50 N, in other words, the current dynamic strength windows are taking shape as 175-200% of the static failure load for 10 Hz and 55 Hz, and 200-225% of the static failure load for 40 Hz. These windows could be refined through further rounds of bisecting the intended force to hone in on the dynamic strength threshold more closely. In addition, the results of which runs and thereby which cases are deemed elastic or plastic is directly dependent on the choice of the plastic threshold with respect to ΔPTD. A full investigation would also require directly analyzing the realized forces per case and correlating that to each individual elastic vs. plastic outcome, to discover the realized dynamic strength. Based on the observation that the alternating force and the most intense negative force (i.e. minimum force) are both typically higher than the intended force, it is reasonable to argue that the achieved dynamic strength windows in these tests is even higher than those based on the intended force. Still, these results provide a first indication of the ballpark ranges for dynamic strength of 6061 aluminum beams under sinusoidal excitation for the given geometry considered.

Transitioning from a primarily PTD-based method to an exploration of the potential for a power-dissipation-based or hysteresis-based approach, the power dissipated per cycle is calculated from the area enclosed by the measured force-velocity loops (e.g., from Figure 4a) [10], as indicated in equation (5):

$$P = \oint_{cyc} v.dF \ . \tag{5}$$

The mean value of the power dissipation of all cycles for each beam, P_{mean}, is plotted versus $|F_{min}|$ in Figure 7 for all beams tested. It can be seen from the data that as the frequency increases, the power dissipation increases, as one would expect. At each frequency, there seems to be a power dissipation threshold, beyond which fracture would occur, as expected.

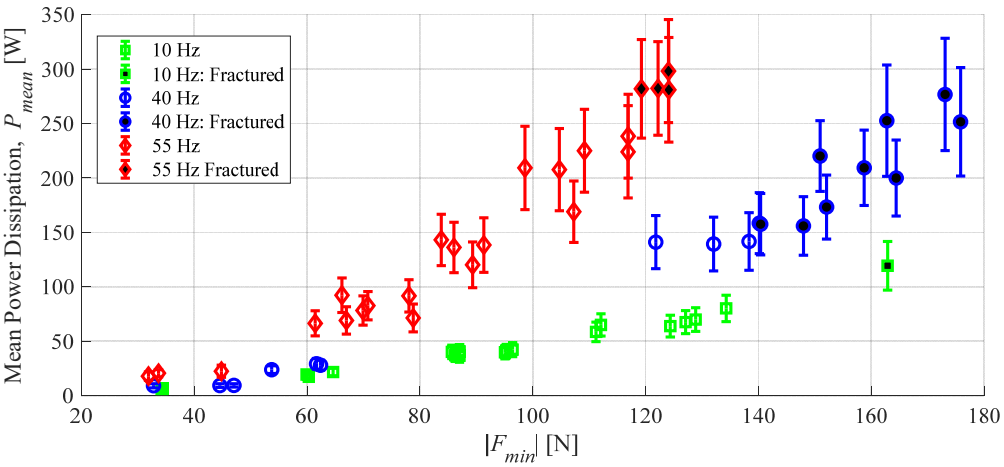

Fig. 7 Mean per-cycle power dissipation versus $|F_{min}|$ for all beams excited at 10, 40, and 55 Hz. Markers indicate the mean of the per-cycle value for a given run and are colored by excitation frequency. Any beams that fractured during the dynamic test are indicated by black-filled markers. Error bars represent +/- one standard deviation in the per-cycle value

Based on an assumption that the dissipative force is proportional to the beam's velocity, the power dissipation should be proprotional to the force squared. The normalized power dissipation, P_n, is then defined as the power disspation per cycle divided by the square of the per cycle alternating force (equation 6).

$$P_n = \frac{P}{F_{alt-cyc}^2} \tag{6}$$

The reasoning behind this analysis is that the onset of plastic deformation should serve as an additional source of energy dissipation, which might cause a deviation in the normalized power dissipation trend. As a first step in exploring this idea, the mean of the normalized power dissipation, $P_{n,\,mean,}$ is plotted against $|F_{min}|$ in Figure 8 for all beams tested.

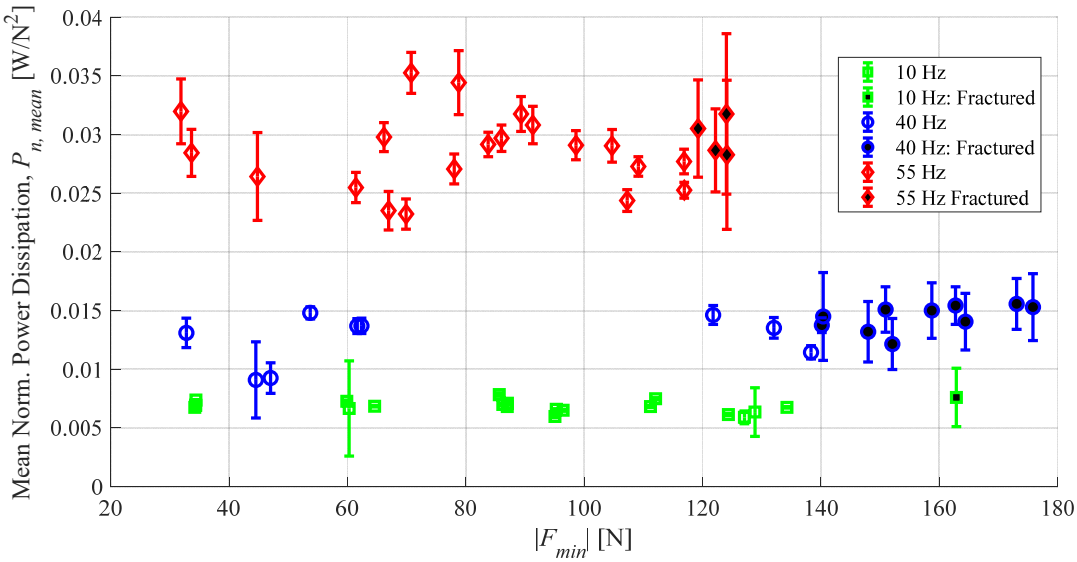

Fig. 8 Mean of the normalized (by the square of the per-cycle alternating force) per-cycle power dissipation versus $|F_{min}|$ for all beams excited at 10, 40, and 55 Hz. Markers are colored by excitation frequency and any beams that fractured during the dynamic test are indicated by black-filled markers. Error bars represent +/- one standard deviation in the per-cycle value

The 55 Hz beams have the highest values of $P_{n,\,mean}$, while the 10 Hz beams have the lowest. The dynamics of the whole system (beam, stinger and shaker stiffness and damping) are expected to affect this parameter. Unlike the power dissipation plot that shows an increase as $|F_{min}|$ increases, the normalized power dissipation seems independent of $|F_{min}|$ but increases as the excitation frequency grows. This increase might be resulting from an increase in the shaker's viscous damping at the higher operational frequencies, or from other increased sources of damping. Still, there does not yet appear to be a clear deviation in plastic cases from elastic cases from this lens, as the fractured cases currently fall within the same normalized power dissipation band. Exploration of this approach and related methodological variations is ongoing.

Another discussion-worthy factor that may influence the results in this study is the amount of PTD_{pre} (pre-test PTD). The tolerance on the straightness of the original beams (i.e. before adding attachment holes) was designated by the manufacturer to be 0.24 degrees. For many cases, the pre-test straightness of the beams did fall within this tolerance. However, the highest PTD_{pre} measurement included in this study, for example, was 1.37 mm, which translates to an angle of approximately 0.34 degrees across the 9-inch (22.9-cm) exposed length of the beam. It is suspected that any straightness deviation above the manufacturing tolerance could be from changes either during the shipping process from the manufacturer to campus or from the in-house manufacturing process to add the two pin holes and one stinger hole. Regardless of the source of "pre-damage," it is hypothesized that a "plastic" test case (i.e. realized forcing amplitude above the dynamic strength of the beam for a given excitation frequency) should still result in a noticeable ΔPTD, due to additional plastic deformation during the cyclic loading. As a first step towards exploring the potential effect of the level of PTD_{pre} on the dynamic strength results, beams for each test were chosen such that various levels of PTD_{pre} were represented in the data from each case. By frequency, overall, the min to max PTD_{pre} (pre-test PTD) ranges across all related runs for 10 Hz, 40 Hz, and 55 Hz tests were 0.07-1.16 mm, 0.01-0.84 mm, and 0.00-1.37 mm, respectively. On the other hand, the median PTD_{pre} values for 10 Hz, 40 Hz, and 55 Hz runs were 0.27 mm, 0.14 mm, and 0.19 mm, respectively. At this stage in the study, the PTD_{pre} does not appear to have a significant effect on the outcome. However, full investigation of the pre-PTD influence is of scientific interest and will be reported on in a future publication.

CONCLUSIONS & FUTURE WORK

The conclusions of this ongoing study thus far are threefold:

(1) A test procedure to characterize the dynamic strength of 6061 aluminum beams under sinusoidal loading for a fixed frequency and 60 seconds of full amplitude excitation was developed.
(2) Different methods to monitor the onset and progression of plastic deformation during these dynamic strength tests via distinguishing between plastic (failed) vs. elastic (survived) loads have been explored, and the top candidates of interest remain as (a) comparing the pre-/pos-test permanent tip deflection (PTD) to assess changes above an estimated measurement error threshold, and (b) exploring characteristic changes in power dissipation density or hysteresis trends.
(3) Data from the 63 completed dynamic tests indicates that the dynamic failure load for each of the three excitation frequencies (10, 40, and 55 Hz) was above the static failure load. Based on the intended applied force as a more conservative measure than the realized peak force, the currently estimated force window in which the dynamic strength lies is 175-200% of the static failure load for 10 Hz and 55 Hz, and 200-225% of the static failure load for 40 Hz.

For ongoing and future work, top priority tasks include (1) continuing tests at more excitation frequencies, (2) performing a robust uncertainty analysis around the sources of error in the testing procedure, especially as it relates to measurement uncertainty for the pre-/post-test PTD check and associated detection threshold for plastic deformation, (3) continuing to explore and finalize plastic deformation monitoring methods (such as the hysteresis-based approach discussed here), and (4) continuing to investigate the effect, if any, of the intensity of pre-test PTD on the dynamic strength results. Once the monitoring methods are finalized and a full set of frequency-dependent data is acquired, the next step is to apply findings from this work to modify structural design practices to take advantage of this avenue for mass mitigation when sizing hardware that will undergo vibratory loading. The engineering labor to size hardware would simply have a higher strength property associated with the dynamic load and would require no additional effort. The proposed modified design approach would be equally applicable to engineering projects in fields that include designs driven by dynamic loads and need light weighted hardware.

ACKNOWLEDGEMENTS

This study was supported by a collaborative agreement with NASA Marshall Space Flight Center (grant number 80NSSC22M0199) in partnership with the NASA Minority University Research and Education Project (MUREP). Complimentary financial support was provided internally by CSUN and the College of Engineering and Computer Science. All testing was performed at CSUN. We would also like to thank the CSUN mechanical engineering faculty and Master's and Bachelor's students who have been part of our larger team: Dr. Christoph Schaal, Dr. Jamie Booth, Hariet Yousefi, Brian Sanchez, and Joseluis Ahumada-Ceja. We would like to thank the CSUN machine shop technicians, Cesar Crisostomo and Neil Mendoza for all of their work to machine custom parts for us. In addition, we would also like to thank Polytec, The Modal Shop, and PCB Piezotronics for their thorough customer support.

REFERENCES

[1] Knight, J. Brent, "Mass Mitigation in Structural Designs via Dynamic Properties," *Challenges in Mechanics of Time Dependent Materials, Mechanics of Biological Systems and Materials & Micro-and Nanomechanics, Volume 2: Proceedings of the 2021 Annual Conference & Exposition on Experimental and Applied Mechanics*, pp 89-95, Springer International Publishing, 2021.
[2] Budynas, R. and J. Nisbett, *Shigley's Mechanical Engineering Design*, New York: McGraw-Hill, 2020.
[3] NASA, *NASA-STD-5001B: Structural Design and Test Factors of Safety for Spacecraft Hardware,* 2022.
[4] NASA Marshall Space Flight Center, *MSFC-HDBK-505: Structural Strength Program Requirements*, 2005.
[5] Fitzka, M., B. M. Schoenbauer, R. K. Rhein, N. Sanaei, S. Zekriardehani, S. A. Tekalur, J. W. Carroll, and H. Mayer, "Usability of Ultrasonic Frequency Testing for Rapid Generation of High and Very High Cycle Fatigue Data," *Materials*, 14(9), pp. 2245, 2021.
[6] Ewins, David J, *Modal testing: theory, practice and application*, John Wiley & Sons, 2009.

[7] Chopra, A. K., *Dynamics of Structures: Theory and Applications to Earthquake Engineering*, Prentice Hall, 1995.
[8] Senseny, P.E., J. Duffy, and R. H. Hawley, "Experiments on Strain Rate History and Temperature Effects During Plastic Deformation on Close-Packet Metals," *Journal of Applied Mechanics*, 45(1), pp. 60-65, 1978.
[9] Klepaczko, J. R. and C. Y. Chiem, "On rate sensitivity of f.c.c. metals, instantaneous rate sensitivity and rate sensitivity of strain hardening," *Journal of the Mechanics and Physics of Solids*, 34(1), pp. 29-54, 1986.
[10] Knight, R. D., *Physics for Scientists and Engineers: A Strategic Approach with Modern Physics*, New York: Pearson, 2013.